Dalton Transactions

RSC Publishing

PAPER

View Article Online
View Journal | View Issue

Cite this: *Dalton Trans.*, 2013, **42**, 207

Synthetic, structural, spectroscopic and theoretical study of a Mn(III)–Cu(II) dimer containing a Jahn–Teller compressed Mn ion†

Nelly Berg,[a] Thomas N. Hooper,[b] Junjie Liu,[c] Christopher C. Beedle,[c] Saurabh Kumar Singh,[d] Gopalan Rajaraman,*[d] Stergios Piligkos,[e] Stephen Hill,*[c,f] Euan K. Brechin*[b] and Leigh F. Jones*[a]

Received 30th August 2012,
Accepted 8th October 2012

DOI: 10.1039/c2dt31995k

www.rsc.org/dalton

The heterobimetallic complex [Cu(II)Mn(III)(L)$_2$(py)$_4$](ClO$_4$)·EtOH (**1**) built using the pro-ligand 2,2′-biphenol (LH$_2$), contains a rare example of a Jahn–Teller compressed Mn(III) centre. Dc magnetic susceptibility measurements on **1** reveal a strong antiferromagnetic exchange between the Cu(II) and Mn(III) ions mediated through the phenolate O-atoms (J = −33.4 cm^{-1}), with magnetisation measurements at low temperatures and high fields suggesting significant anisotropy. Simulations of high-field and high frequency powder EPR data suggest a single-ion anisotropy $D_{Mn(III)}$ = +4.45 cm^{-1}. DFT calculations also yield an antiferromagnetic exchange for **1**, though the magnitude is overestimated (J_{DFT} = −71 cm^{-1}). Calculations reveal that the antiferromagnetic interaction essentially stems from the Mn($d_{x^2-y^2}$)–Cu($d_{x^2-y^2}$) interaction. The computed single-ion anisotropy and cluster anisotropy also correlates well with experiment. A larger cluster anisotropy for the S = 3/2 state compared to the single-ion anisotropy of Mn(III) is rationalised on the basis of orbital mixing and various contributions that arise due to the spin–orbit interaction.

Introduction

Coordination chemistry regularly provides examples of fascinating homo- and heterometallic molecules with potential applications in disparate fields. In bioinorganic chemistry certain heterometallic manganese complexes have been proposed as biomimetic models for energy and electron transfer processes – one such stimulus being the [Mn$_4$CaO$_4$] cubane-like catalytic unit within photosystem II (PSII).[1] Mn has also played a pivotal role in the field of molecular magnetism: the anisotropic nature of the Mn(III) ion means that it is regularly selected as the metal of choice in the synthesis of Single-Molecule Magnets (SMMs)[2] and Single-Chain Magnets (SCMs),[3] whilst the isotropic Mn(II) ion can be employed in the construction of molecular magnetic refrigerants.[4] Molecular Nanomagnetism has also seen a renaissance in the synthesis of heterometallic 3d/4f cluster compounds, driven, in the main, by the tunable anisotropy of the lanthanide ions,[5,6] offering the chemist the opportunity to vary the physical properties of a molecule without significantly altering structure. Similarly the systematic synthesis of the extensive family of heterometallic [Cr$_7$M] wheels and their many siblings has made elegant in-roads into the field of quantum information processing *via* molecular qubits.[7]

The dissemination of these wonderfully elaborate and complex polynuclear heterometallic architectures was of course preceded by fundamental studies of the magnetic exchange between metal ions in very simple complexes, such as homo- and hetereometallic dimers. An early example of this was the heterobimetallic complex [CuVO(fsa)$_2$en] (where (fsa)$_2$en^{4-} is the ligand derived from *N*,*N*′-(2-hydroxy-3-carboxybenzylidene)-1,2-diaminoethane) in which the nature of the intramolecular ferromagnetic exchange was explained by the orthogonality of the magnetic orbitals centred on the Cu(II) and V(IV) ions.[8] More recently the heterodinuclear complex [Cu(II)Mn(III)Cl(5-Br-sap)$_2$(MeOH)] (where 5-Br-sap = 5-bromo-

[a]*School of Chemistry, National University of Ireland, Galway, University Road, Galway, Ireland. E-mail: leigh.jones@nuigalway.ie; Tel: +353 091-49-3462*
[b]*EaStCHEM School of Chemistry, The University of Edinburgh, West Mains Road, Edinburgh, EH9 3JJ, UK. E-mail: ebrechin@staffmail.ed.ac.uk*
[c]*National High Magnetic Field Laboratory, Florida State University, Tallahassee, FL 32310, USA*
[d]*Department of Chemistry, Indian Institute of Technology, Powai, Mumbai, 400076, India. E-mail: rajaraman@chem.iitb.ac.in*
[e]*Department of Chemistry, University of Copenhagen, Universitetsparken 5, DK-2100, Denmark. E-mail: piligkos@kiku.dk*
[f]*Department of Physics, Florida State University, Tallahassee, FL 32306, USA. E-mail: shill@magnet.fsu.edu*

†Electronic supplementary information (ESI) available. CCDC 898371. For ESI and crystallographic data in CIF or other electronic format see DOI: 10.1039/c2dt31995k

2-salicylideneamino-1-propanol) was shown to exhibit ferromagnetic exchange, with the magnetic anisotropy stemming from the presence of the single Jahn–Teller elongated Mn(III) ion conferring SMM behaviour.[9]

Herein we present the synthesis, structure, magnetism and theoretical study of the rather unusual heterobimetallic complex $[Cu(II)Mn(III)(L)_2(py)_4](ClO_4)\cdot EtOH$ (**1**) constructed using the pro-ligand 2,2′-biphenol (LH_2) which contains a rare example of a Jahn–Teller compressed Mn(III) ion.[10]

Results and discussion

Complex **1** is readily prepared *via* the reaction of Mn(II)-$(ClO_4)_2\cdot 6H_2O$, anhydrous Cu(I)Cl, 2,2′-biphenol (LH_2) and $NEt_4(OH)$ in a EtOH/pyridine solvent mixture. The resultant green/black solution, upon filtration and slow evaporation, gives rise to X-ray diffraction quality crystals of **1** in ~20% yield (see Table S1† for crystallographic data). Crystals were in a triclinic cell and structure solution was performed in the space group $P\bar{1}$.

The structure of the cation in **1** (Fig. 1) comprises a single distorted square planar Cu(II) ion (Cu1) linked to a single six coordinate Jahn–Teller compressed Mn(III) ion (Mn1) by two bridging O_{phen} donor atoms (Mn1–O1–Cu1, 99.72°; Mn1–O3–Cu1, 101.28°) belonging to two distinct doubly deprotonated 2,2′-biphenolate ligands. Their remaining O_{phen} atoms (O2 and O4) are terminally bonded, providing the short axial bonds to the sole Mn(III) ion that define the Jahn–Teller compressed axis (Mn1–O2, 1.880 Å; Mn1–O4, 1.871 Å). The longer equatorial bonds range between 2.051 Å (Mn1–O3) and 2.205 Å (Mn1–N4). The "free" axial sites of the square planar Cu(II) ion are blocked by the presence of the phenyl rings of the rather twisted L^{2-} ligands (Cu···Ph(centroid) = 3.560–3.579 Å); indeed the dihedral angles between the Ph rings on these same ligands are 49.86° [C5–C8] and 51.60° [C17–C20] respectively. Four terminal pyridine ligands complete the coordination spheres at the six coordinate Mn(III) centre (N3 and N4) and at the four coordinate Cu(II) site (N1 and N2) affording $\{MnO_4N_2\}$ and $\{CuO_2N_2\}$ coordination spheres, respectively.

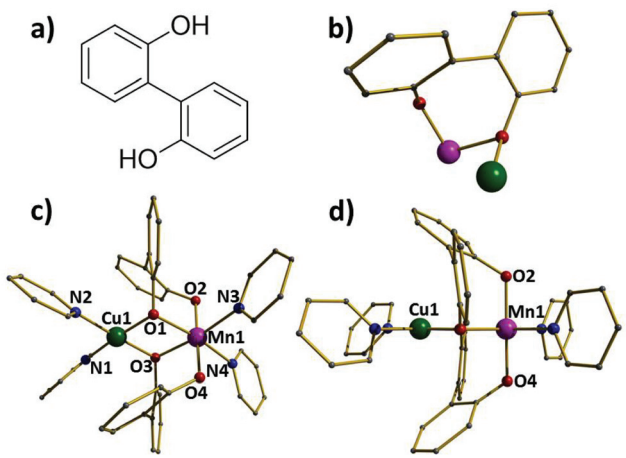

Fig. 1 (a) The pro-ligand 2,2′-biphenol (LH_2) and (b) its coordination mode upon double deprotonation. Molecular structure of the heterobimetallic cation in **1** as viewed off-set (c) and perpendicular (d) to the Jahn–Teller compressed axis of the Mn(III) ion. Colour code: green (Cu), purple (Mn), red (O), blue (N) and grey (C). Hydrogen atoms and counter anions have been omitted for clarity.

The resultant $\{Cu(II)Mn(III)(L)_2(py)_4\}^+$ cation is charge balanced by the presence of a single ClO_4^- ion. The latter H-bonds to a EtOH molecule of crystallisation (O8···O9, 2.827 Å), with the closest contacts to the cluster complex being O5···H28 = 2.570 Å and O5···H29 = 2.600 Å. The ethanol molecule of crystallisation also hydrogen bonds to an aromatic proton (H26) of a nearby pyridine ligand (O9···H26, 2.759 Å). In the crystal the individual $\{Cu(II)Mn(III)(L)_2(py)_4\}^+$ cluster units pack in superimposable rows along the *a* unit cell direction and are separated at a M···M distance of ~12 Å. These 1D rows pack in the common brickwork formation in the *bc* plane (Fig. S1†).

Although a number of Cu(II)–Mn(II) dinuclear complexes are known in the literature,[11] a CSD search reveals that **1** is one of very few examples to show the Cu(II)–Mn(III) oxidation state distribution,[9,12] and is indeed the first to possess a Mn(III) ion exhibiting a Jahn–Teller compression. Complex **1** is structurally very similar to the aforementioned $[Cu(II)Mn(III)Cl(5\text{-Br-sap})_2(MeOH)]$ (**2**). Both contain $[Cu(II)(OR)_2Mn(III)]$ magnetic cores (albeit with different R-groups), resulting in very similar Cu(II)–O(R)–Mn(III) bond angles (99.71 and 101.26° in **1**) and (102.1° in **2**). Indeed the only difference in terms of magnetic structure is the presence of a Jahn–Teller compressed Mn(III) ion in **1** and a Jahn–Teller elongated Mn(III) ion in **2**. The synthesis of **1** therefore represents an ideal opportunity to investigate the magneto-structural relationship in this family of complexes (*vide infra*).

SQUID magnetometry

Dc magnetic susceptibility measurements were performed on a powdered microcrystalline sample of **1** in an applied magnetic field of 0.1 T and in the temperature range 250 to 5 K. The results are plotted as the $\chi_M T$ product *vs.* T in the top panel of Fig. 2. The high temperature $\chi_M T$ value of 2.270 cm^3 K mol^{-1} is lower than that expected from the spin-only value (3.375 cm^3 K mol^{-1}) for non-interacting high-spin Mn(III) ($3d^4$) and Cu(II) ($3d^9$) ions, assuming g = 2. This reflects the existence of a strong intramolecular antiferromagnetic interaction in **1**. The $\chi_M T$ product decreases in a sigmoidal-like fashion with decreasing temperature until it reaches a plateau of around 1.75 cm^3 K mol^{-1} in the 45 to 20 K temperature interval. The $\chi_M T$ product at this low temperature plateau is consistent with the existence of a thermally isolated S = 3/2 spin-state. For the modelling of the $\chi_M T$ product we used spin-Hamiltonian (1):

$$\hat{H} = -2J\hat{S}_{Cu}\cdot\hat{S}_{Mn} + D_{Mn}[\hat{S}^2_{z,Mn} - S_{Mn}(S_{Mn}+1)/3] + \mu_B \sum_{i=Cu,Mn}\{g_i\vec{B}\cdot\vec{S}_i\} \quad (1)$$

where J is the Cu(II)–Mn(III) isotropic exchange interaction parameter, $\hat{S}$ is a spin-operator, D_{Mn} is the single-ion uniaxial

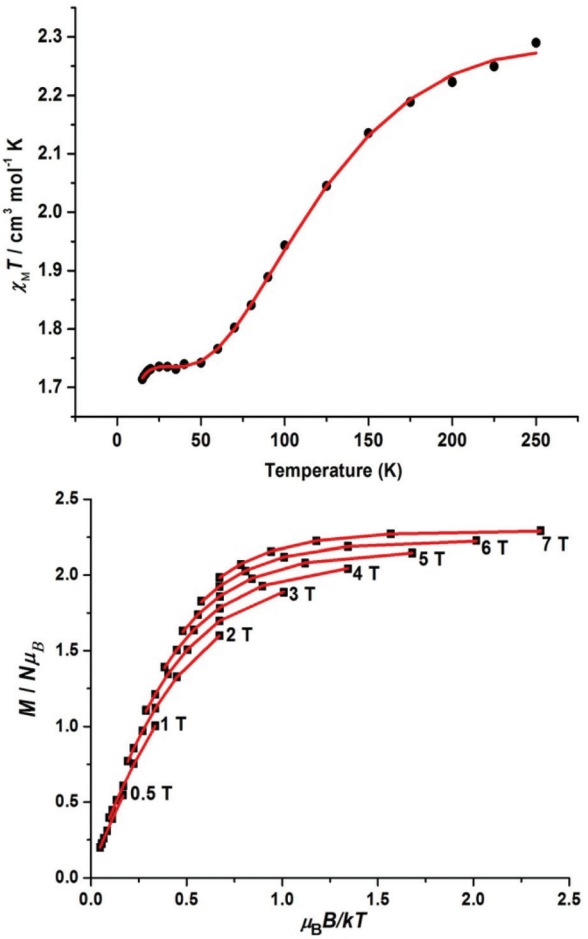

Fig. 2 Upper panel: plot of the $\chi_M T$ product of **1** *vs.* T in the 250–5 K temperature range in an applied field of 0.1 T. The solid red line is the best-fit of the data with $J = -33.4$ cm^{-1} as described in the text. Lower panel: plot of reduced magnetisation of **1** in the 2.0 to 7.0 K temperature range and at the indicated field strengths. The solid red lines are the best-fit of the data with J fixed to -33.4 cm^{-1} and $D_{Mn} = +4.95$ cm^{-1}, as described in the text.

anisotropy of Mn(III), $S = 2$ is the single-ion spin of Mn(III), μ_B is the Bohr magneton, $g_{Mn} = 2.0$ and $g_{Cu} = 2.1$ are the employed isotropic g-factors of the Mn(III) and Cu(II) ions, respectively, and $\vec{B}$ is the applied magnetic field vector. The $\chi_M T$ product of **1** was numerically fitted by use of the simplex algorithm[13] to spin-Hamiltonian (1) by numerical diagonalisation of the spin-Hamiltonian matrix of dimension 10 by 10. While fitting the $\chi_M T$ product, it became apparent that inclusion of the Mn(III) single-ion anisotropy term does not significantly improve the quality of fit, as measured by the χ^2 statistics. This is as expected since anisotropy effects are predominant at very low temperatures and thus, do not weight significantly in the fitting of the $\chi_M T$ product. The best-fit parameter of (1) to the $\chi_M T$ product of **1** was $J = -33.4$ cm^{-1}, affording an $S = 3/2$ spin ground state with the $S = 5/2$ excited state some 167 cm^{-1} higher in energy. In addition, inter-molecular interactions were taken into account in the frame of mean-field theory, by use of the Curie–Weiss temperature, θ. A Curie–Weiss constant of $\theta = -0.9$ K, was necessary to reproduce the small drop of the $\chi_M T$ product below ~20 K. The determined strong antiferromagnetic interaction is consistent with the above qualitative description of the thermal dependence of the $\chi_M T$ product of **1**.

In order to determine, by magnetisation measurements, the single-ion axial anisotropy parameter for the Mn(III) centre in **1**, variable-temperature-variable-field magnetisation measurements were performed in the $T = 2.0$–7.0 K and $B = 0.5$–7.0 T temperature and dc magnetic field ranges, respectively. These experimental data are presented as reduced magnetisation ($M/N\mu_B$ *vs.* $\mu_B B/kT$, with N being Avogadro's number and k the Boltzmann constant) in the lower panel of Fig. 2. They were again numerically fitted, by use of the simplex algorithm,[13] to spin-Hamiltonian (1), by numerical diagonalisation of the 10 by 10 spin-Hamiltonian matrix. The best fit parameter, keeping J fixed to -33.4 cm^{-1} (as determined by fitting the $\chi_M T$ product), was $D_{Mn} = +4.95$ cm^{-1}. Forcing the D_{Mn} parameter to vary only in the negative-value semi-axis, leads to χ^2 values that are two orders of magnitude higher than the ones obtained by letting D_{Mn} vary freely to give $D_{Mn} = +4.95$ cm^{-1}. The positive value of D_{Mn} is in good agreement with the axially compressed nature of the coordination sphere of the Mn(III) ion.

EPR spectroscopy

Powder EPR data were collected for complex **1** in order to determine the magnetic anisotropy of the dimer. Given the spin states of the constituent ions ($S = 2$ and 1/2 for Mn(III) and Cu(II) respectively), one expects a half integer ground state spin of either $S = 3/2$ or 5/2 for the dimer. The low-energy spectrum should thus consist of either two or three [*i.e.* $(2S + 1)$] Kramers doublets, split by any associated magnetic anisotropy. Fig. 3 displays representative frequency-dependent powder EPR spectra for complex **1** collected between 100.6 and 406 GHz at a relatively low temperature of 5 K. All of the labelled resonances persist to the lowest temperatures investigated (not shown), indicating that they involve transitions either within or from the lowest Kramers doublet. At frequencies below 200 GHz, the spectra are dominated by three strong resonance branches that we assign to the x, y and z-transitions within the ground-state Kramers doublet; these are marked by open red, blue and black circles, respectively. As can be seen in the frequency *versus* field map in Fig. 4, the peak positions corresponding to these transitions each lie on simulated curves (*vide infra*) that intersect the origin, as expected for intra-Kramers transitions. At frequencies above 200 GHz, additional resonance branches appear at low fields (solid black squares and circles). As can be seen in Fig. 4, these resonances all lie on lines/curves that meet at a unique finite-frequency offset on the zero-field axis. We thus assign them as inter-Kramers transitions, and the intercept on the ordinate corresponds exactly to the zero-field energy splitting between the two lowest Kramers doublets. We note that this splitting of 381 ± 5 GHz is rather substantial for a complex comprised of just Mn(III) and Cu(II) ions. The solid circles in Fig. 4 correspond to the usual $\Delta m_s = \pm 1$ perpendicular-mode EPR

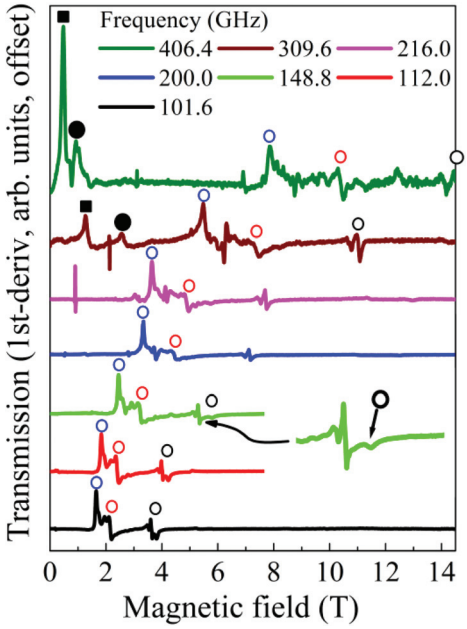

Fig. 3 Representative frequency dependent powder EPR spectra collected at 5 K: the red, blue and black open circles denote the intra-Kramers *x*, *y* and *z*-components of the spectra, while the solid circles ($\Delta m_s = \pm 1$) and squares ($\Delta m_s = \pm 2$) denote transitions between Kramers doublets; the inset displays an expanded portion of the 148.8 GHz spectrum in the vicinity of the *z*-component (see main text for explanation). The extremely sharp features seen in some of the spectra (*e.g.* at ~1 T in the 216 GHz spectrum) correspond to known signals from oxygen adsorbed in the sample holder.

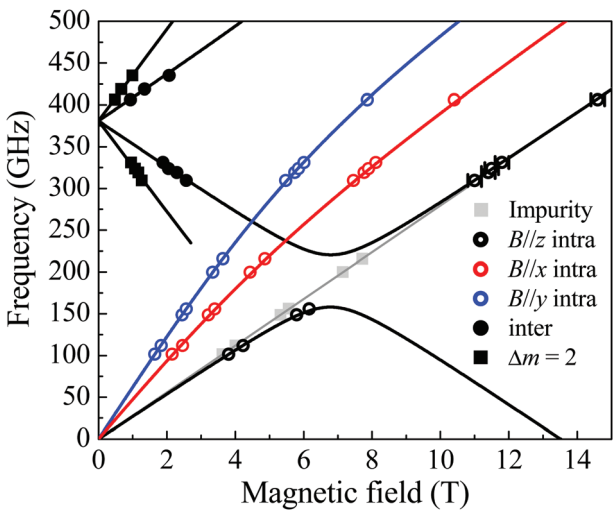

Fig. 4 Plot of the frequency dependent EPR peak positions as a function of the applied magnetic field strength. The solid curves (same colour coding as the data) correspond to the simulations described in the main text. Note that the grey data points and the grey line correspond to an impurity signal with $g = 2.003(2)$.

transitions, while the solid squares correspond to $\Delta m_s = \pm 2$ resonances (see below). The simulations assume that the applied field, B, is parallel to z. However, all three inter-Kramers components (*i.e.* $B//x$, y and z) generate $\Delta m_s = \pm 1$ and ± 2 resonances at similar locations, provided the applied field is relatively weak (<3 T), which may account for the appreciable intensity of the lowest field 406.4 GHz peak in Fig. 3.

While analysis of susceptibility data enables reliable estimates of the exchange coupling within a simple spin system, especially a dimer, EPR measurements provide much more robust constraints on both the sign and magnitude of the magneto-anisotropy. The EPR data presented in Fig. 4 clearly reveal the presence of a pair of low-energy Kramers doublets. However, they do not rule out the possibility of a third higher-lying doublet. Thus, a determination of the ground state spin from the EPR data is not entirely straightforward. This would require careful analysis of much weaker transitions observed at elevated temperatures, and we do not pursue this here because the susceptibility measurements clearly indicate that the coupling within the dimer is antiferromagnetic. Therefore, in the following analysis, we assume that the ground state spin value is $S = 3/2$. In doing so, we will see that the obtained anisotropy is quite consistent with expectations, thus providing indirect confirmation of the $S = 3/2$ ground state spin value.

We first turn our attention to the sign of the second-order axial zero-field splitting parameter D_S associated with the $S = 3/2$ ground state. In the presence of easy-plane type anisotropy ($D_S > 0$), the $B//x$- and y-components of the spectrum associated with the lowest Kramers doublet (red and blue circles, respectively, Fig. 4) possess effective g-values that are substantially larger than 2.00, *i.e.* slopes that substantially exceed 28 GHz T^{-1} as $B \rightarrow 0$; meanwhile, the $B//z$-component has an effective g-value (slope) very close to 2.00 (or 28 GHz T^{-1}, denoted by the grey line in Fig. 4). The opposite holds for the easy-axis case ($D < 0$).[14,15] Thus, the powder EPR data clearly support the presence of an easy-plane type anisotropy ($D > 0$), which one would expect in a JT compressed Mn(III) system, since this represents the main source of anisotropy within the dimer. The magnitude of D_S is approximately constrained by the intercept of the inter-Kramers resonance branches. For a purely axial system, this intercept corresponds exactly to $2D_S$, hence $D_S \approx 381/2$ GHz = 6.35 cm^{-1}. However, as can clearly be seen from Fig. 3 and 4, there is a considerable splitting between the x and y components of the spectrum, signifying a rhombic distortion and, hence, a rhombic E_S parameter. In such situations, D_S can only be determined precisely *via* diagonalisation of the following effective spin Hamiltonian:

$$\hat{H}_S = D_S \hat{S}_z^2 + E_S(\hat{S}_x^2 - \hat{S}_y^2) + \mu_B \vec{B} \cdot \vec{\vec{g}}_S \cdot \hat{S} \qquad (2)$$

where $\hat{S}$ represents the total spin operator and $\hat{S}_i$ ($i = x, y, z$) its components, the subscript $S = 3/2$ defines the total spin-state on which the effective spin-Hamiltonian (2) is applied and g_S is the Landé tensor of the total spin-state S. The best simulation of the data in Fig. 4 was obtained with the following parameters: $D_S = +6.27$ cm^{-1}, $E_S = \pm 0.57$ cm^{-1}, $g_{S,x} = 1.97$, $g_{S,y} = 1.97$ and $g_{S,z} = 1.98$. The main constraint on the E_S parameter is the splitting between the x- and y-components of the intra-Kramers transitions (red and blue curves in Fig. 4), *i.e.* its value is well constrained. While one might expect a corresponding difference between $g_{S,x}$ and $g_{S,y}$, this leads to an over

parameterization of the model. Therefore, we have assumed these parameters to have the same value.

The transverse anisotropy (E) leads naturally to an avoided-crossing between the $m_S = -3/2$ and $m_S = +1/2$ components of the two Kramers doublets, which meet at ~7 T when $B//z$. It is this interaction that is the reason for the ~60 GHz (2 cm^{-1}) gap between the inter- and intra-Kramers z-component resonance branches at ~7 T in Fig. 4 (solid black lines). Surprisingly, spectra recorded at frequencies close to 200 GHz (*e.g.* the blue curve in Fig. 3) still show weak resonances in this gapped region of the $B//z$ simulations. Closer inspection of the spectra reveals that the z component appears to consist of a narrow derivative (*i.e.* a sharp peak followed by a sharp minimum) superimposed on a broad dip; this contrasts the x and y components that each consist of a single feature, *i.e.* a peak for y and a shoulder for x, as expected for such a powder spectrum. The narrow and broad z-components are separately plotted in Fig. 4 as grey squares and open black circles. The sharp components lie on a straight (grey) line passing through the origin, having a slope corresponding to $g = 2.003(2)$. At most frequencies, the broad dip lies very close to this line. However, one clearly sees that the broad component moves appreciably to the high-field side of the $g = 2.003$ position (the sharp peak) as the frequency approaches the gapped region; the relevant portion of the 148.8 GHz spectrum has been enlarged in Fig. 3 (green curve) to emphasize this point. Indeed, if one assumes that it is this broad dip that corresponds to the z-component of the dimer spectrum, one finds excellent agreement with the simulations in Fig. 4. Meanwhile, we believe that the sharp component corresponds to an impurity phase within the powder, possibly containing isotropic Mn(II); this is often found to be the case in Mn-containing polynuclear clusters, and explains why a resonance is still observed in the gapped region of the $B//z$ spectrum. In fact, it is notable that the 200 GHz spectrum exhibits only a sharp component, the broad dip appears to be absent, which is why an open circle is not included in Fig. 4 for this frequency.

Due to the strong Cu(II)–Mn(III) exchange interaction ($J \sim -33$ cm^{-1}), we can make a reliable estimation of the anisotropy parameters associated with the individual ions using the projection method.[16] According to Kramers' theorem, any zero-field splitting interaction associated with the Cu(II) ion ($S_{Cu} = 1/2$) is strictly forbidden; hence, the zero-field splitting parameters of the molecule are determined only by the anisotropy parameters of the Mn(III) ion. The projection method gives $\ddot{D}_{S=3/2} = 1.4\,\ddot{D}_{Mn}$, where $\ddot{D}_{S=3/2}$ and $\ddot{D}_{Mn}$ are the anisotropy tensors of the ground spin-state and the Mn(III) ion, respectively. Therefore, we estimate that $D_{Mn} = +4.45$ cm^{-1} and $E_{Mn} = \pm 0.41$ cm^{-1}. We note that these zero-field interaction parameters obtained *via* EPR data are in excellent agreement with the parameters obtained *via* the reduced magnetisation measurements, and are consistent with values found for related single-ion Mn(III) compounds (see Table S3† and references therein).[17] Finally, we comment on the g-values obtained from the EPR measurements. Again, using projection methods, one can estimate that $\ddot{g}_{S=3/2} = 1.2\,\ddot{g}_{Mn} - 0.2\,\ddot{g}_{Cu}$.

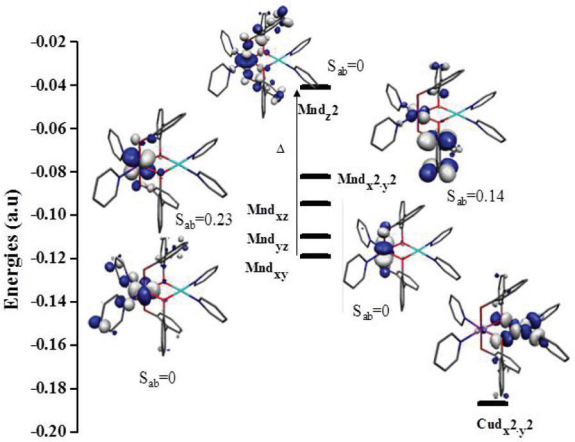

Fig. 5 DFT calculated magnetic orbitals of Mn(III) and Cu(II) with computed S_{ab} (overlap integral) values. The isodensity surface represented corresponds to a value of 0.05 e$^-$/bohr^3.

Consequently, the obtained g-values for the $S = 3/2$ ground spin-state should be dominated by the Mn(III) ion, which is consistent with the obtained values that are very close to 2.00.

DFT analysis

Density functional studies have been performed on complex **1** to compute the J value and to explore the origin of the nature of the interaction observed experimentally. The B3LYP/TZV combination (see computational details below) yields a J value of −71 cm^{-1}. Although the sign of J has been correctly reproduced, the magnitude is overestimated compared to experiment ($J_{exp} = -33.4$ cm^{-1}). Although the employed methodology generally offers good numerical estimates of J values, there are instances where overestimation of the J has been noted.[18,19] Calculations performed incorporating the counter-anion did not lead to any significant improvement (−71 cm^{-1} *vs.* −83 cm^{-1}; Table S5†). Since our aim is to probe the origin of antiferromagnetic coupling in the {MnCu} pair, we have analysed the wave function and the magnetic orbitals of the Mn(III) and Cu(II) ions (Fig. 5).

The Cu(II) ion is in a square planar environment, with the unpaired electron residing in the $d_{x^2-y^2}$ orbital (b_{1g}). For Mn(III) the following configuration has been detected from the computed wave function: $b_{2g}(d_{xy})^1 e_g(d_{xz})^1 e_g(d_{yz})^1 b_{1g}(d_{x^2-y^2})^1$ where the $a_{1g}(d_z^2)$ orbital is found to be empty and lies 1.12 eV higher in energy than the b_{1g} orbital. This splitting is related to the strength of the distortion and significant splitting demonstrates that the Mn(III) ion is undergoing relatively strong JT compression.[20,21]

Qualitatively $\Delta(E_{dxy} - E_{dz^2})$ – calculated to be ~2.12 eV for **1** (Fig. 5) – is related to the anisotropy by the following equation for a Jahn–Teller compressed Mn(III) ion:

$$D = D_{zz} - \frac{(D_{xx} + D_{yy})}{2} \approx +\frac{3\zeta_{eff}^2}{16\Delta} \qquad (3)$$

where ζ_{eff} is the effective covalently reduced one-electron spin–orbit coupling (SOC) constant of the metal ion under

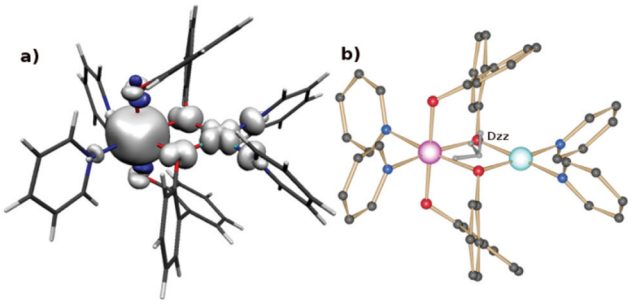

Fig. 6 (a) DFT computed spin density plot of **1** for the $S = 2$ state. The isodensity surface represented corresponds to a value of 0.005 $e^-/bohr^3$. The white and blue regions indicate positive and negative spin populations, respectively. (b) DFT calculated orientation of *D*-tensor in **1**. H-atoms have been omitted for clarity.

investigation, and Δ is as defined in Fig. 5. Since in both the metal ions the $b_{1g}(d_{x^2-y^2})$ orbital is singly occupied, a significant interaction between these two magnetic orbitals is expected, leading to antiferromagnetic coupling. To prove this hypothesis, overlap integrals between pairs of magnetic orbitals have been computed. Our overlap integral analysis reveals a significant overlap between Mn($d_{x^2-y^2}$) and Cu($d_{x^2-y^2}$) (Table S6†). Additionally Mn(d_{xz}) has non-negligible overlap with the Cu($d_{x^2-y^2}$) orbital. The Mn($d_{x^2-y^2}$)–Cu($d_{x^2-y^2}$) interaction is very significant (Fig. 5) and this leads to a moderate antiferromagnetic interaction in complex **1**. The other dinuclear {MnCu} (**2**) complex reported in the literature has ferromagnetic coupling.[9a] In that complex the Mn(III) is Jahn–Teller elongated the $d_{x^2-y^2}$ orbital is empty and the significant Mn($d_{x^2-y^2}$)–Cu($d_{x^2-y^2}$) interaction present in **1**, is absent, leading to moderate ferromagnetic coupling. This pair of complexes illustrates rather nicely how the magnetic coupling can be tuned from ferromagnetic to antiferromagnetic by altering the nature of the distortion (elongation *vs.* compression) on the Mn(III) site.

The spin density values on the Mn(III) (1.663) and Cu(II) (0.59) ions clearly indicates strong spin delocalisation to other atoms. The spin densities on the bridging O-atoms (O1 and O3) are found to be positive (0.11 and 0.12) while the N-atoms coordinated to Cu(II) and Mn(III) are also found to have positive spin densities. On the other hand, the spin densities on the O-atoms lying in the axial direction are found to be negative (Fig. 6). This is in line with our expectation where the empty d_z^2 orbital propagates spin polarization rather than spin delocalization. Such a mixture of delocalization and polarization has been reported previously.[19c,22]

We have also computed the ZFS parameter of complex **1** using the methodology established by Neese *et al.*[21] We have performed calculations on complex **1** and also on a fictitious {MnZn} model complex of **1** to estimate the $S = 3/2$ ZFS of **1** and the $S = 2$ single-ion anisotropy of the Mn(III) ion, in order to compare to the experimentally extracted parameters. The calculated single-ion anisotropy of the Mn(III) ion is +1.94 cm^{-1}, while the cluster anisotropy is computed to be +2.35 cm^{-1}. The HF-EPR estimates of the ZFS are +4.45 and +6.27 cm^{-1}, respectively. Our DFT calculations reproduce the sign and the trend correctly, but clearly underestimate the magnitude quite considerably. Such underestimation by DFT methods has been well documented: accurate reproduction demands inclusion of exited state contributions and this is possible only by means of *ab initio* calculations.[21]

Table 1 DFT computed spin-flip/spin-conserved excitations for the {MnCu} and {MnZn} complexes

Spin flip excitations	Single ion anisotropy (cm^{-1})	Cluster anisotropy (cm^{-1})
SOMO–SOMO α → β	1.215	1.484
DOMO–SOMO β → β	0.028	0.059
SOMO–VMO α → α	0.339	−2.729
DOMO–VMO β → α	0.002	3.554

Analysis of the contributions to the net *D*-tensor suggest the main source arises from spin–orbit coupling (D_{SOC}), while the spin–spin contribution (D_{SS}) is found to be small, and significantly less than that reported for complexes in which the Mn(III) ion is Jahn–Teller elongated.[20,21] The significant contributions to the ZFS are listed in Table 1. For D_{SOC} the spin-flip excitations account for nearly 65% of the contribution. Multiple contributions to the *D*-tensor listed in Table 1 reveal some distinct differences between the single-ion and the cluster anisotropy. The α → β (spin-up to spin-down) excitations are pronounced for the Mn(III) single-ion ($S = 2$ state) anisotropy, while other contributions are very small. However for the dinuclear {MnCu} compound ($S = 3/2$ ground state), very large β → α and α → α contributions were detected, in addition to the expected α → β spin flip. A large β → α and α → α for the antiferromagnetically coupled dimer is expected due to the mixing of Mn^{III} and Cu^{II} d-orbitals. The mixing is evident from the computed overlap integrals and the discussed spin density distribution. An in depth analysis to understand the contribution of various terms to the ZFS can only be obtained through an *ab initio* CASSCF/PT2 studies.[17d]

Analysing the wave function (see Fig. 5 and related discussion on Δ) reveals that the main reason for the difference is that the Mn(III) ion has one empty α type orbital (for the $S = 3/2$ ground state) and this leads to large singly occupied molecular orbital (SOMO) to virtual molecular orbitals (VMO) contribution. There is also a significant contribution due to doubly occupied orbitals (DOMO) to VMO due to the presence of Cu(II). These two contributions are minimal for the mononuclear Mn(III) ions. This is illustrated in Fig. 7. It is apparent from the break-up contributions given for the {MnCu} complex that the DOMO → VMO excitation which has the largest positive value determines the net sign of the anisotropy. Since this parameter is related to the mixing of Mn and Cu d-orbitals, efforts to vary the ligand field are expected to significantly affect the magnitude of the anisotropy. The computed *D*-tensor orientation for the {MnCu} complex is shown in Fig. 6. As expected the D_{zz} axis is aligned along JT axis with a deviation of approximately 5° (Table 2).

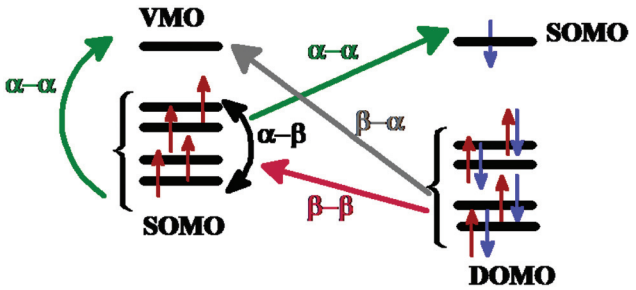

Fig. 7 Schematic diagram illustrating the different contribution to anisotropy in complex **1**.

Table 2 Experimental *versus* DFT computed single-ion and cluster anisotropies with SOC and SS contributions

Complex	D total (cm^{-1})	D_{SOC} (cm^{-1})	D_{SS} (cm^{-1})	E/D	g-tensor
DFT on **1** (S = 3/2)	2.35	2.369	−0.009	0.06	1.98
DFT on {MnZn}	1.94	1.58	0.35	0.06	1.99
HF-EPR on **1**	6.27			0.09	—
HF-EPR Mn(III) ion	4.78			0.08	1.98

Conclusions

Reaction of anhydrous CuCl, $Mn(ClO_4)_2{\cdot}6H_2O$ and 2,2-biphenol (LH_2) in an EtOH/pyridine solvent mixture produces the heterobimetallic complex $[Cu(II)Mn(III)(L)_2(py)_4](ClO_4){\cdot}EtOH$ (**1**·EtOH). Complex **1** is a rare example of a dimeric [Cu(II)Mn(III)] cluster compound and the first example to exhibit a Jahn–Teller compressed Mn(III) centre. Magnetic susceptibility and magnetisation studies conclude that the exchange in **1** is antiferromagnetic resulting in an isolated S = 3/2 ground spin state, with J = −33.4 cm^{-1}, g = 2.0 and $D_{Mn(III)}$ = +4.95 cm^{-1}. High-field, high-frequency EPR studies on powdered samples of **1** corroborate these findings, giving rise to the spin Hamiltonian parameters $D_{Mn(III)}$ = +4.45 cm^{-1} and $E_{Mn(III)}$ = +0.41 cm^{-1}. DFT calculations offer insights into the mechanism of magnetic coupling where the origin of the antiferromagnetic interaction is related to the nature of the Jahn–Teller distortion. Calculations also yield a reasonable estimate of the anisotropy for complex **1** and explain how the mixing of the Mn(III) and Cu(II) d-based orbitals leads to dramatic changes in the sign as well as the magnitude of the anisotropy for **1**.

Experimental section

Physical measurements

Infra-red spectra were recorded on a Perkin Elmer FT-IR *Spectrum One* spectrometer equipped with a Universal ATR Sampling accessory (NUI Galway). Elemental analyses were carried out by the School of Chemistry microanalysis service at NUI Galway. Variable-temperature, solid-state direct current (dc) magnetic susceptibility data down to 5 K were collected on powdered samples using a Quantum Design MPMS-XL SQUID magnetometer equipped with a 7 T dc magnet (University of Edinburgh). Diamagnetic corrections were applied to the observed paramagnetic susceptibilities using Pascals' constants. Complex **1** was set in eicosane to avoid torqueing of the crystallites. Powder EPR data were collected in a transmission-type spectrometer employing a 17 T superconducting magnet. A phase-locked oscillator, in conjunction with a series of multipliers and amplifiers, was employed as a microwave source capable of providing quasi-continuous frequency coverage up to 600+ GHz; a cold bolometer was used for detection.[23]

Computational details

DFT calculations combined with the Broken Symmetry (BS) approach[24] were employed to compute the J values. The BS method has a proven record of yielding good numerical estimates of J constants for a variety of complexes.[25,26] A detailed technical discussion of the computational details can be found elsewhere.[27,28] Here, we have performed most of our calculations using the Gaussian 09 suite of programs with the fragment approach.[29] We have employed a hybrid B3LYP functional[30] with TZV basis sets on all atoms.[31] A very tight SCF convergence was employed throughout. DFT calculations for the estimation of the D-tensor used the ORCA suite of programmes,[32] employing the non-hybrid BP86 functional[33] using quasi-degenerate theory[34] with CP approach.[35,36] The Alhrichs TZVPPP basis set was used for the Mn(III) and Cu(II) ions, while for the remaining atoms we have used the TZVP basis set. The RI approximations were considered during calculation with auxiliary TZV/J columbic fitting basis set.[37] Increased integration grids (Grid 5 in ORCA convention) along with tight SCF convergence were used.

Materials and syntheses

All reactions were performed under aerobic conditions and all reagents and solvents were used as purchased. ***Caution***: Although we encountered no problems care should be taken when using the potentially explosive perchlorate salts. The $NEt_4(OH)$ solution employed was a 40% by weight aqueous solution which was used as purchased.

$[Cu(II)Mn(III)(L)_2(py)_4](ClO_4){\cdot}EtOH$ (1)

$Mn(ClO_4)_2{\cdot}6H_2O$ (0.25 g, 0.98 mmol) and anhydrous Cu(I)Cl (0.39 g, 3.94 mmol) were dissolved in 35 cm^3 EtOH along with 1 cm^3 of pyridine. 2,2′-biphenol (LH_2) (0.73 g, 3.94 mmol) was then added along with 2 drops of $NEt_4(OH)$. The resultant solution was stirred for 5–7 minutes before being filtered to give a green/black solution. Brown block-like crystals of **1** were obtained in ~20% yield upon slow evaporation of the mother liquor over a period of 24 hours. *Note: Attempts at repeating the reaction employing Cu(II) salts have all been unsuccessful.* Elemental analysis calculated (found) (%) for $C_{45}H_{40}N_4O_9ClMnCu$ (**1**·EtOH): C: 57.82 (57.98), H: 4.31 (3.81),

N: 5.99 (6.05). FT-IR (cm^{-1}): 3508.2(w), 3043.5(w), 2970.4(w), 1605.5(m), 1585.3(w), 1484.2(m), 1465.7(m), 1446.4(m), 1432.4(m), 1288.4(w), 1272.5(w), 1250.0(m), 1213.6(m), 1153.7(w), 1080.7(vs), 1066.8(vs), 1043.2(s), 1015.6(m), 956.7(w), 940.4(w), 869.4(w), 852.8(m), 833.7(m), 756.0(vs), 731.3(m), 695.1(vs).

X-ray crystallography

The structure of **1** was collected on an Xcalibur S single crystal diffractometer (Oxford Diffraction) using an enhanced Mo source. Each data reduction was carried out on the CrysAlisPro software package. For more detailed refinement information please consult the ESI. Full details can also be found in the CIF file: CCDC 898371.

Acknowledgements

We wish to thank the NUI Galway Millennium Fund (LFJ) and the Irish Research Council (IRCSET Embark Initiative (NB)). EKB wishes to thank the Leverhulme Trust and the EPSRC. Work at the National High Magnetic Field Laboratory is supported by NSF Cooperative Agreement no. DMR-0654118 and by the State of Florida. SH acknowledges the support of the NSF (CHE0924374) and SP the Danish Natural Science Research Council (FNU) for a Sapere Aude Fellowship (10-081659). GR would like to acknowledge financial support from the Government of India through Department of Science and Technology (SR/S1/IC-41/2010) and Indian Institute of Technology Bombay for computing time and a JRF position (SKS).

Notes and references

1 See for example: (*a*) V. K. Yachandra, V. J. DeRose, M. J. Latimer, I. Mukerji, K. Sauer and M. P. Klein, *Science*, 1993, **260**, 675; (*b*) V. J. DeRose, I. Mukerji, M. J. Latimer, V. K. Yachandra, K. Sauer and M. P. Klein, *J. Am. Chem. Soc.*, 1994, **116**, 5239; (*c*) G. Aromí, M. W. Wemple, S. J. Aubin, K. Folting, D. N. Hendrickson and G. Christou, *J. Am. Chem. Soc.*, 1998, **120**, 5850; (*d*) T. Wydrzynski and S. Satoh, *Photosystem II: The Light-Driven Water: Palstpoquinone Oxidoreductase*, Springer, Dordrecht, The Netherlands, 2005; (*e*) J. Yano and V. K. Yachandra, *Inorg. Chem.*, 2008, **47**, 1711.

2 (*a*) G. Aromí and E. K. Brechin, *Struct. Bonding*, 2006, **122**, 1; (*b*) M. Murrie and D. J. Price, *Annu. Rep. Prog. Chem., Sect. A*, 2007, **103**, 20; (*c*) A. K. Boudalis, Y. Sanakis, C. P. Raptopoulou and V. Psycharis, *Magnetism and Superconductivity in Low-Dimensional Systems: Utilization in Future Applications*, ed. D. Stamopoulos, Nova Science Publishers Inc., New York, 2008, pp. 1–77; (*d*) G. Christou, *Polyhedron*, 2005, **24**, 2065; (*e*) *Molecular Cluster Magnets*, ed. R. E. P. Winpenny, World Scientific Books, Singapore, 2011.

3 (*a*) C. Coulon, H. Miyasaka and R. Clérac, *Struct. Bonding*, 2006, **122**, 163; (*b*) L. Bogani, A. Vindigni, R. Sessoli and D. Gatteschi, *J. Mater. Chem.*, 2008, **18**, 4750; (*c*) H.-L. Sun, Z.-M. Wang and S. Gao, *Coord. Chem. Rev.*, 2010, **254**, 1081; (*d*) R. Lescouëzec, L. M. Toma, J. Vaissermann, M. Verdaguer, F. S. Delgado, C. Ruiz-Perez, F. L. Lloret and M. Julve, *Coord. Chem. Rev.*, 2005, **249**, 2691; (*e*) R. Clérac, H. Miyasaka, M. Yamashita and C. Coulon, *J. Am. Chem. Soc.*, 2002, **124**, 12837; (*f*) M. Ferbinteanu, H. Miyasaka, W. Wernsdorfer, K. Nakata, K. Sugiura, M. Yamashita, C. Coulon and R. Clérac, *J. Am. Chem. Soc.*, 2005, **127**, 3099.

4 (*a*) M. Evangelisti and E. K. Brechin, *Dalton Trans.*, 2010, **39**, 4672; (*b*) M. Evangelisti, F. Luis, L. J. de Jongh and M. Affronte, *J. Mater. Chem.*, 2006, 2534.

5 See for example: (*a*) R. Sessoli and A. K. Powell, *Coord. Chem. Rev.*, 2009, **253**, 2328; (*b*) T. C. Stamatatos, S. J. Teat, W. Wernsdorfer and G. Christou, *Angew. Chem., Int. Ed.*, 2009, **48**, 521; (*c*) M. N. Akhtar, V. Mereacre, G. Novitchi, J.-P. Tuchagues, C. E. Anson and A. K. Powell, *Chem.–Eur. J.*, 2009, **15**, 7278; (*d*) J.-L. Liu, F.-S. Guo, Z.-S. Meng, Y.-Z. Zheng, J.-D. Leng, M.-L. Tong, L. Ungur, L. F. Chibotaru, K. J. Heroux and D. N. Hendrickson, *Chem. Sci.*, 2011, **2**, 1268; (*e*) J.-P. Costes, F. Dahan and A. Dupuis, *Inorg. Chem.*, 2000, **39**, 5994; (*f*) M. Andruh, J.-P. Costes, C. Diaz and S. Gao, *Inorg. Chem.*, 2009, **48**, 3342; (*g*) G. Karotsis, S. Kennedy, S. J. Teat, C. M. Beavers, D. A. Fowler, J. J. Morales, M. Evangelisti, S. J. Dalgarno and E. K. Brechin, *J. Am. Chem. Soc.*, 2010, **132**, 12983; (*h*) E. Colacio, J. Ruiz-Sanchez, F. J. White and E. K. Brechin, *Inorg. Chem.*, 2011, **50**, 7268.

6 (*a*) J. Rinck, G. Novitchi, W. Van den Heuvel, L. Ungur, Y. Lan, W. Wernsdorfer, C. E. Anson, L. F. Chibotaru and A. K. Powell, *Angew. Chem., Int. Ed.*, 2010, **49**, 7583; (*b*) A. Yamashita, A. Watanabe, S. Akine, T. Nabeshima, M. Nakano, T. Yamamura and T. Kajiwara, *Angew. Chem., Int. Ed.*, 2011, **50**, 1; (*c*) T. Peristeraki, M. Samios, M. Siczek, T. Lis and C. J. Milios, *Inorg. Chem.*, 2011, **50**, 5175; (*d*) T. N. Hooper, J. Schnack, S. Piligkos, M. Evangelisti and E. K. Brechin, *Angew. Chem., Int. Ed.*, 2012, **51**, 4633; (*e*) C. E. Burrow, T. J. Burchell, P.-H. Lin, F. Habib, W. Wernsdorfer, R. Clérac and M. Murugesu, *Inorg. Chem.*, 2009, **48**, 8051.

7 (*a*) M. Affronte, S. Carretta, G. A. Timco and R. E. P. Winpenny, *Chem. Commun.*, 2007, 1789; (*b*) G. A. Timco, T. B. Faust, F. Tuna and R. E. P. Winpenny, *Chem. Soc. Rev.*, 2011, **40**, 3067; (*c*) T. B. Faust, V. Bellini, A. Candini, S. Carretta, G. Lorusso, D. R. Allan, L. Carthy, D. Collison, R. J. Docherty, J. Kenyon, J. Machin, E. J. L. McInnes, C. A. Muryn, H. Nowell, R. G. Pritchard, S. J. Teat, G. A. Timco, F. Tuna, G. F. S. Whitehead, W. Wernsdorfer, M. Affronte and R. E. P. Winpenny, *Chem.–Eur. J.*, 2011, **17**, 14020–14030; (*d*) C. F. Lee, D. A. Leigh, R. G. Pritchard, D. Schultz, S. J. Teat, G. A. Timco and R. E. P. Winpenny, *Nature*, 2009, **458**, 314; (*e*) G. A. Timco, S. Carretta, F. Troiani, F. Tuna, R. J. Pritchard, C. A. Muryn, E. J. L. McInnes, A. Ghirri, A. Candini, P. Santini, G. Amoretti, M. Affronte and R. E. P. Winpenny, *Nat. Nanotechnol.*, 2009, **4**, 173.

8 (*a*) O. Kahn, *Inorg. Chim. Acta*, 1982, **62**, 3; (*b*) O. Kahn, J. Galy, Y. Journaux, J. Jaud and I. Morgenstern-Badarau, *J. Am. Chem. Soc.*, 1982, **104**, 2165; (*c*) O. Kahn, *Molecular Magnetism*, VCH, Weinheim, 1993.

9 (*a*) H. Oshio, M. Nihei, A. Yoshida, H. Nojiri, M. Nakano, A. Yamaguchi, Y. Karaki and H. Ishimoto, *Chem.–Eur. J.*, 2005, **11**, 843; (*b*) M. Nihei, A. Yoshida, S. Koizumi and H. Oshio, *Polyhedron*, 2007, **26**, 1997.

10 For examples of the coordination chemistry of 2,2′-biphenol (LH_2) see: (*a*) N. Berg, S. M. Taylor, A. Prescimone, E. K. Brechin and L. F. Jones, *CrystEngComm*, 2012, **14**, 2732; (*b*) N. Berg, T. Rajeshkumar, S. M. Taylor, E. K. Brechin, G. Rajaraman and L. F. Jones, *Chem.–Eur. J.*, 2012, **18**, 5906; (*c*) N. Berg and L. F. Jones, *CrystEngComm*, 2011, **13**, 5510; (*d*) A. R. Schake, E. A. Schmitt, A. J. Conti, W. E. Strieb, J. C. Huffman, D. N. Hendrickson and G. Christou, *Inorg. Chem.*, 1991, **30**, 3192; (*e*) D. P. Goldberg, A. Caneschi, C. D. Delfs, R. Sessoli and S. J. Lippard, *J. Am. Chem. Soc.*, 1995, **117**, 5789.

11 (*a*) C. J. O'Connor, D. P. Freyberg and E. Sinn, *Inorg. Chem.*, 1979, **18**, 1077; (*b*) H. Okawa, J. Nishio, M. Ohba, M. Tadokoro, N. Matsumoto, M. Koikawa, S. Kida and D. E. Fenton, *Inorg. Chem.*, 1993, **32**, 2949; (*c*) C. Fraser, R. Ostrander, A. L. Rheingold, C. White and B. Bosnich, *Inorg. Chem.*, 1994, **33**, 324; (*d*) A. Hori, Y. Mitsuka, M. Ohba and H. Okawa, *Inorg. Chim. Acta*, 2002, **337**, 113; (*e*) L. Bo, Z. Hong, P. Zhi-Quan, S. You, W. Cheng-Gang, Z. Han-Ping, H. Jing-Dong and C. Ru-An, *J. Coord. Chem.*, 2006, **569**, 1271.

12 (*a*) F. Birkelbach, M. Winter, U. Florke, H.-J. Haupt, C. Butzlaff, M. Lengen, E. Bill, A. X. Trautwein, K. Wieghardt and P. Chaudhuri, *Inorg. Chem.*, 1994, **33**, 3990; (*b*) Z.-W. Li, P.-P. Yang, L.-C. Li and D.-Z. Liao, *Inorg. Chim. Acta*, 2009, **362**, 3381.

13 W. H. Press, S. A. Teukolsky, W. T. Vetterling and B. P. Flannery, *Numerical Recipes in C: The Art of Scientific Computing*, Cambridge University Press, Cambridge, 2nd edn, 1992.

14 J. M. Zadrozny, J. Liu, N. A. Piro, C. J. Chang, S. Hill and J. R. Long, *Chem. Commun.*, 2012, **48**, 3927.

15 X. Feng, J. Liu, T. D. Harris, S. Hill and J. R. Long, *J. Am. Chem. Soc.*, 2012, **134**, 7521.

16 A. Bencini and D. Gatteschi, *Electron Paramagnetic Resonance of Exchange Coupled Clusters*, Springer, Berlin, 1990.

17 For examples of J–T compressed mononuclear Mn(III) complexes see: (*a*) C. Mantel, A. K. Hassan, J. Pecaut, A. Deronzier, M.-N. Collomb and C. Duboc-Toia, *J. Am. Chem. Soc.*, 2003, **125**, 12337–12344; (*b*) J. Krzystek, G. J. Yeagle, J.-H. Park, R. D. Britt, M. W. Meisel, L.-C. Brunel and J. Tesler, *Inorg. Chem.*, 2003, **42**, 4610–4618; (*c*) Q. Scheifele, C. Riplinger, F. Neese, H. Weihe, A.-L. Barra, F. Juranyi, A. Podlesnyak and P. L. W. Tregenna-Piggott, *Inorg. Chem.*, 2009, **47**, 439–447; (*d*) S. Romain, C. Duboc, F. Neese, E. Rivière, L. R. Hanton, A. G. Blackman, C. Philouze, J.-C. Leprêtre, A. Deronzier and M.-N. Collomb, *Chem.–Eur. J.*, 2009, **15**, 980–988.

18 E. Ruiz, S. Alvarez, A. Rodriguez-Fortea, P. Alemany, Y. Pouillon and C. Massobrio, in *Magnetism: Molecules to Materials*, ed. J. S. Miller and M. Drillon, Wiley-VCH, Weinheim, 2001, vol. II.

19 (*a*) A. Abu-Nawwas, J. Cano, P. Christian, T. Mallah, G. Rajaraman, S. J. Teat, R. E. P. Winpenny and Y. Yasuhiko, *Chem. Commun.*, 2004, 314; (*b*) G. Rajaraman, J. Cano, E. K. Brechin and E. J. L. McInnes, *Chem. Commun.*, 2004, 1476; (*c*) G. Rajaraman, M. Murugesu, M. Soler, W. Wernsdorfer, M. Helliwell, S. J. Teat, G. Christou and E. K. Brechin, *J. Am. Chem. Soc.*, 2004, **126**, 15445.

20 J. Cirera, E. Ruiz, S. Alvarez, F. Neese and J. Kortus, *Chem.–Eur. J.*, 2009, **15**, 4078.

21 (*a*) D. Maganas, S. Sottini, P. Kyritsis, E. J. J. Groenen and F. Neese, *Inorg. Chem.*, 2011, **50**, 8741; (*b*) C. Duboc, D. Ganyushin, K. Sivalingam, M.-N. Collomb and F. Neese, *J. Phys. Chem. A.*, 2010, **114**, 10750; (*c*) F. Neese, *J. Am. Chem. Soc.*, 2006, **128**, 10213.

22 L. F. Jones, G. Rajaraman, J. Brockman, M. Murugesu, J. Raftery, S. J. Teat, W. Wernsdorfer, G. Christou, E. K. Brechin and D. Collison, *Chem.–Eur. J.*, 2004, **10**, 5180.

23 R. Herchel, R. Boča, J. Krzystek, A. Ozarowski, M. Dura and J. van Slageren, *J. Am. Chem. Soc.*, 2007, **129**, 10306.

24 L. Noodleman, *J. Chem. Phys.*, 1981, **74**, 5737.

25 (*a*) E. Ruiz, S. Alvarez, J. Cano and P. Alemany, *J. Comput. Chem.*, 1999, **20**, 1391; (*b*) E. Ruiz, A. R. Fortea, J. Cano, S. Alvarez and P. Alemany, *J. Comput. Chem.*, 2003, **24**, 982; (*c*) E. Ruiz, J. Cano, S. Alvarez, A. Caneschi and D. Gatteschi, *J. Am. Chem. Soc.*, 2003, **152**, 6791; (*d*) G. Rajaraman, J. Cano, E. K. Brechin and E. J. L. McInnes, *Chem. Commun.*, 2004, 1476.

26 S. Piligkos, G. Rajaraman, M. Soler, N. Kirchner, J. van Slageren, R. Bircher, S. Parsons, H. Güdel, J. Kortus, W. Wernsdorfer, G. Christou and E. K. Brechin, *J.Am. Chem. Soc.*, 2005, **127**, 5572.

27 P. Christian, G. Rajaraman, A. Harrison, M. Helliwell, J. J. W. McDouall, J. Raftery and R. E. P. Winpenny, *Dalton Trans.*, 2004, 2550.

28 E. Ruiz, S. Alvarez, A. Rodriguez-Fortea, P. Alemany, Y. Pouillon and C. Massobrio, in *Magnetism: Molecules to Materials*, ed. J. S. Miller, M. Drillon, Wiley-VCH, Weinheim, 2001, vol. II, p. 227.

29 M. J. Frisch, G. W. Trucks, H. B. Schlegel, G. E. Scuseria, M. A. Robb, J. R. Cheeseman, G. Scalmani, V. Barone, B. Mennucci, G. A. Petersson, H. Nakatsuji, M. Caricato, X. Li, H. P. Hratchian, A. F. Izmaylov, J. Bloino, G. Zheng, J. L. Sonnenberg, M. Hada, M. Ehara, K. Toyota, R. Fukuda, J. Hasegawa, M. Ishida, T. Nakajima, Y. Honda, O. Kitao, H. Nakai, T. Vreven, J. A. Montgomery Jr., J. E. Peralta, F. Ogliaro, M. Bearpark, J. J. Heyd, E. Brothers, K. N. Kudin, V. N. Staroverov, R. Kobayashi, J. Normand, K. Raghavachari, A. Rendell, J. C. Burant, S. S. Iyengar, J. Tomasi, M. Cossi, N. Rega, J. M. Millam, M. Klene, J. E. Knox, J. B. Cross, V. Bakken, C. Adamo, J. Jaramillo,

R. Gomperts, R. E. Stratmann, O. Yazyev, A. J. Austin, R. Cammi, C. Pomelli, J. W. Ochterski, R. L. Martin, K. Morokuma, V. G. Zakrzewski, G. A. Voth, P. Salvador, J. J. Dannenberg, S. Dapprich, A. D. Daniels, Ö. Farkas, J. B. Foresman, J. V. Ortiz, J. Cioslowski and D. J. Fox, *Gaussian 09 (Revision A.1)*, Gaussian, Inc., Wallingford, CT, 2009.

30 A. D. Becke, *J. Chem. Phys.*, 1993, **98**, 5648.

31 A. Schafer, C. Huber and R. Ahlrichs, *J. Chem. Phys.*, 1994, **100**, 5829.

32 ORCA 2.9.0 F. Neese, 2012.

33 (*a*) J. P. Perdew, *Phys. Rev. B: Condens. Matter*, 1986, **33**, 8822; (*b*) A. D. Becke, *Phys. Rev. A*, 1988, **38**, 3098.

34 D. Ganyushin and F. Neese, *J. Chem. Phys.*, 2006, **125**, 024103.

35 F. Neese, *J. Chem. Phys.*, 2007, **127**, 164112.

36 K. Ray, A. Begum, T. Weyhermuller, S. Piligkos, J. van Slageren, F. Neese and K. Wieghardt, *J. Am. Chem. Soc.*, 2005, **127**, 4403.

37 F. Weigend, *Phys. Chem. Chem. Phys.*, 2006, **8**, 1057.

